Journal of Materials Chemistry A

Crystallised mesoporous TiO2(A)-VO2(M/R) nanocomposite films with self-cleaning and excellent thermochromic properties

Journal:	*Journal of Materials Chemistry A*
Manuscript ID:	TA-ART-04-2014-001585.R1
Article Type:	Paper
Date Submitted by the Author:	05-May-2014
Complete List of Authors:	Chen, Zhang; SICCAS, Gao, Yanfeng; Shanghai institute of Ceramics, Cao, Chuanxiang; SICCAS, Chen, Shi; SICCAS, ; Shanghai institute of Ceramics, Luo, Hongjie; SICCAS, ; Shanghai institute of Ceramics,

Crystallised mesoporous TiO_2(A)-VO_2(M/R) nanocomposite films with self-cleaning and excellent thermochromic properties

Zhang Chen,[1] Chuanxiang Cao,[1] Shi Chen,[1] Hongjie Luo,[1,2] and Yanfeng Gao[1,2]*

1 State Key Laboratory of High Performance Ceramics and Superfine Microstructure, Shanghai institute of Ceramics, Chinese Academy of Sciences, 1295 Dingxi, Shanghai 200050, China

2 School of Materials Science and Engineering, Shanghai University, 99 Shangda, Shanghai 200444, China

* Author for correspondence. Email: yfgao@shu.edu.ac.cn

Tel/Fax: +86-21-6990-6218

Abstract

VO_2 (M/R) (Monoclinic/Rutile) shows a reversible insulator-metal transition (IMT) near room temperature and is a widely used film material for thermochromic smart windows. Recent studies have shown that VO_2-based nanocomposite coatings show better optical performance (luminous transmittance, T_{lum} and solar energy modification ability, ΔT_{sol}) than pure VO_2 thin films. In previous studies, we have succeeded in preparing VO_2-based organic-inorganic (O-I) composite coatings and optimising their optical performance to a higher level than ever been reported previously. Compared to O-I composite coatings, inorganic-inorganic (I-I) composite coatings show advantages in weatherability and multifunction (for example, self-cleaning TiO_2-VO_2 composites). In this work, we succeeded in dispersing VO_2 nanoparticles (NPs) in TiO_2 sol by surface modification, and prepared high quality I-I nanocomposite films with comparable optical performance to the best pure VO_2 thin film. With the help of thermal analysis, a two-step annealing process was developed, and crystallised TiO_2(A)(anatase)-VO_2(M/R) composite films were obtained. By introducing mesopores, the optical performance was improved to T_{lum}=62.0 % (20 ºC), 60.5 % (90 ºC) and ΔT_{sol}=14.6 %, better than any reported VO_2-based pure films. Additionally, due to the crystallised TiO_2(A), these composite films show self-cleaning properties (low contact angle and photocatalytic decomposition of organic contaminants).

1. Introduction

VO_2 (M/R) (Monoclinic/Rutile) is the key material in thermochromic smart windows for its reversible insulator-metal transition (IMT) near room temperature[1-5] (VO_2 is used in items instead of VO_2(M/R) if there are no special demands). TiO_2 is a widely used photocatalytic material because of its relatively high quantum yield and elevated stability[6-10]. In the field of VO_2-based thermochromic smart windows, TiO_2 is also an important composite layer because of its good compatibility and similar crystalline structure to that of VO_2[11]. It has been reported that TiO_2 films were effective underneath layers or cover layers to induce the crystallisation of VO_2(M/R)[12, 13], construct a heterostructure for photoemission[14-16], enhance the oxidisation durability[17, 18], regulate the phase transition properties[13, 19-21] and improve the optical performance of VO_2[2, 22-24], and so forth. Compared to these TiO_2-VO_2 multi-layered structures, single-layered composite films are more attractive for their easy preparation, mixing homogeneity of the two components, and most importantly, they display NIR modulation behaviour at much shorter wavelengths than that of typical thin films of pure VO_2, thus show advantages in T_{lum} and ΔT_{sol}[25](also see **S1**). However, only a few studies have been reported, and even fewer studies been performed on smart window usage or optical performances. Films for smart window usage require good thermochromic performance, and methods are available to obtain single-layered TiO_2(A)-VO_2 by simultaneously depositing TiO_2 and VO_2 at critical temperature[26-29], but the diffusion of Ti atoms into VO_2 crystal lattices has always weakened the thermochromic performance of VO_2[26, 30]. Because the crystallisation temperature of TiO_2(A) is much lower than that of VO_2(R)[31], a workable method for TiO_2(A)&VO_2 single-layered composite films could be one that we call the "two-step method": VO_2 nanoparticles (NPs) were first prepared and dispersed in titanium sol, formed a composite film and were then annealed for TiO_2 crystallisation. This method largely restricted Ti diffusion and maintained the thermochromic performance of VO_2.

Previous works have succeeded in the preparation of fine crystalline VO_2 NPs with an average size range from 25-45 nm, and they could be well dispersed in polyurethane[32], laying a foundation for this "two-step method". However, there are still some problems: 1) dispersion of VO_2 NPs in TiO_2 sol, 2) control of TiO_2 crystallisation during annealing and 3) improving the optical performance of the composite films. Detailed descriptions follow:

1) The dispersing method for organic-inorganic (O-I) composite coatings that was reported previously[33] is no longer available. The thickness (d) of these inorganic-inorganic (I-I) composite films is limited because the films would crack during shrinking in the sol-gel process (d<500 nm in our experiment, while I-I composite films can be 3-4 μm or more). Thus, a related high solid content of VO_2 NPs is required for the same T_{lum} and ΔT_{sol} as that of I-I composite. In this situation, a much higher dispersing degree of NPs is required for the inorganic TiO_2-VO_2 composite films.

2) TiO_2(A) is required for its better catalytic performance. However, it has been reported that V atoms would restrict the crystallisation of TiO_2(A) and facilitate rutile TiO_2(TiO_2(R))[34, 35]. Additionally, the degree of diffusion of Ti atoms during annealing is still uncertain because of the high activity of amorphous TiO_2. No similar works could be found, and it is still unknown whether there is a process that can obtain crystalline TiO_2(A)-VO_2 composite film.

3) Optical performance is always been a key feature of VO_2-based smart windows. Although TiO_2-VO_2 composite films have advantages in mechanical strength and weatherability, their optical performance is weakened compared to I-I coatings because of the high refractive index of TiO_2 (**S1**). Methods should be developed to compensate for this weakness.

In this work, we used titanate coupling agent, which is the component of TiO_2 sol used for the surface treatment of TiO_2 NPs. The surface-modified VO_2 (M/R) NPs showed excellent dispersion in the TiO_2 sol

and the formed composite sol had good film-forming properties. By studying the decomposition and crystallisation of TiO_2 and TiO_2-VO_2 xerogels during the annealing process, we obtained TiO_2(A)-VO_2 composite films with T_{lum}≈58% and ΔT_{sol}=5.4%. Furthermore, the optical performance was improved to T_{lum}=62.0 % (20 ºC), 60.5 % (90 ºC) and ΔT_{sol}=14.6 % by introducing mesopores to reduce the refractive index of the composite film. The obtained composite films had low contact angles (less than 5 º for the best sample) and obvious photocatalytic ability as expected.

2. Experiments and Characterisation

2.1 Experiments

VO_2 NPs were prepared with a previously released method. Vanadium pentoxide (V_2O_5, analytically pure) and diamide hydrochloride (N_2H_4•HCl, analytically pure) were employed as starting materials to prepare a VO_2^+ solution. Concentrated HCl (6 mL, 38%) and a solution containing 1 g of N_2H_4•HCl were added into an aqueous suspension (20 mL) containing 3.5 g of V_2O_5. The solution was treated with a small amount of V_2O_5 or N_2H_4•HCl until it contained no VO_2^+ or V^{3+} and was then filtered to form a clear VO^{2+} solution (pH≈1), then stirred for 10 min and transferred to an 18 mL stainless steel autoclave. The hydrothermal reaction was carried out at 370 ºC for 15 h with a heating rate of about 40 °Cmin^{-1}. The final black product was separated by centrifugation and washed once with 40 mL water and twice with 40 mL ethanol.

TiO_2 sol was prepared using tetraisopropoxide (TIPT), deionized water (the pH was adjusted to 1.10 with hydrochloride) and absolute ethanol at the volume ratio of 1:12:0.063. The concentrations of Ti^{4+} were about 0.4 mol·L^{-1}. The obtained solution was aged in closed glass containers at 60 °C for two days.

Dispersing of VO_2 NPs: VO_2 NPs (0.3g) were grinded under the protection of the fresh TiO_2 sol (10ml) for 10 min, and then sealed, ultrasonic dispersed for 60 min and kept high speed stirring for 3 day at 60 °C.

Films preparation: The TiO_2 sols with VO_2 NPs were ultrasonic dispersed for 10 min before used. Films were coated on clean fused-silica substrates by spin-coating of 180 μL of solution with different speed (typically 2000 rad/min), then dried at 100 °C for 2 hours. Films were annealed in a nitrogen atmosphere with designed heating rate and temperature. Mesoporous films were obtained by adding Pluronic P123 ($PEO_{20}PPO_{70}PEO_{20}$, AMW = 5800) in the solution (1-4 wt. % of the TiO_2 sols with VO_2 NPs).

2.2 Characterisation

The morphologies of the samples were determined by transmission electron microscopy (TEM, JEM2010 and JEM 4000EX, JEOL, Tokyo, Japan) and scanning electron microscopy (SEM, Magellan 400, FEI, Hillsboro, America). The crystalline phases of the nanoparticles were determined by X-ray diffraction (XRD, Model D / Max 2550 V, Rigaku, Japan). The optical transmittance characteristics were monitored on a Hitachi U-4100 UV-visible-near-IR spectrophotometer equipped with a film heating unit in the wavelength range of 350–2600 nm. The temperature was measured using a thermocouple in contact with the films, which was controlled through a temperature-control unit. The annealing process of the xerogel was investigated by thermogravimetry/differential thermal analysis (TG-DTA, STA 449C, Netzsch, Selb, Germany) coupled with a Balzers Thermostar^{TM} quadrupole mass spectrometer (MS) at a heating rate of 10 ºC/min. The contact angles of the films were measured with a contact angle apparatus (Chengde Dingsheng Testing Machine Co. Ltd, JY-82A). Surface roughness was calculated from atomic force microscope (AFM, Nanocute SII, Seiko, Japan) data of a 10 × 10 um region.

3. Results and discussion

3.1 Dispersion of VO_2 NPs

According to the study of Langlet, two reactions occurred during the formation of TiO_2 sol[36]. As showing in **Scheme 1 a**, first, isopropoxy groups of TIPT were replaced with ethoxy groups when titanium isopropoxide was diluted in ethanol, forming titanium ethoxide. Then, polymerisation of titanium ethoxide occurred gradually through ageing under the catalysis of H_2O and HCl. Because of the limited amount of water, titanium ethoxide was partly hydrolysed, and the formed polymers were entangled with many ethoxy groups, which contributed to a uniform and stable TiO_2 sol.

The dispersion of VO_2 NPs in the TiO_2 sol is the key to forming a layer of the entangled polymer on the surface of the VO_2 NPs, which would improve their compatibility with the solvent (mixture of ethanol and 2-propanol) and prevent the NPs' aggregation. According to the formation process of TiO_2 sol and the reported surface modification process with the silane coupling agent[37], the tousled layer may be formed as follows (**scheme 1 b**): first, titanium ethoxide reacts with the surface hydroxyl groups of the VO_2 NPs[38], forming a substratum, and then other titanium ethoxide reacts with this substratum layer under the catalysis of H_2O and HCl. If well-dispersed VO_2 NPs are required, VO_2 NPs should be well separated to provide sufficient surface area for the reaction of surface hydroxyl groups with titanium ethoxide, and the reaction between the tousled polymer layers between VO_2 NPs should be restricted to avoid VO_2 NP aggregation.

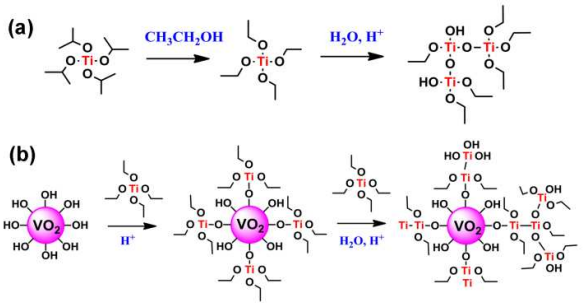

Scheme 1 The processes of TiO_2 sol formation (a) and surface modification of VO_2 NPs (b)

During the experiments, sufficient grinding and ultrasonic dispersion were used to destroy the soft agglomerations of VO_2 NPs; the solutions were sealed (waterproofing), and high-speed stirring was maintained to restrict the reaction between the tousled polymer layers of VO_2 NPs. After 3 days' aging, a TiO_2 sol with well-dispersed VO_2 NPs was formed (**Figure 1 a** and **b,** before and after surface modification, respectively). TEM images (**Figure 1 c**) show that the NPs were separated with a 5-7 nm entangled layer on the surface. The compositional scanning TEM curves of single VO_2 NPs show that the contents of Ti and C were slightly higher on the surface than inside the VO_2 NPs (**Figure 1 d**), which confirms that the surface entangled layer is the polycondensate of titanium ethoxide. Films prepared by spin-coating using this solution are uniform; SEM images of film cross-sections show that VO_2 NPs are uniformly distributed in the TiO_2 gel matrix (**Figure 1 e**). Moreover, the films also show comparable optical performance to that of pure single VO_2 films (see **Table 1**).

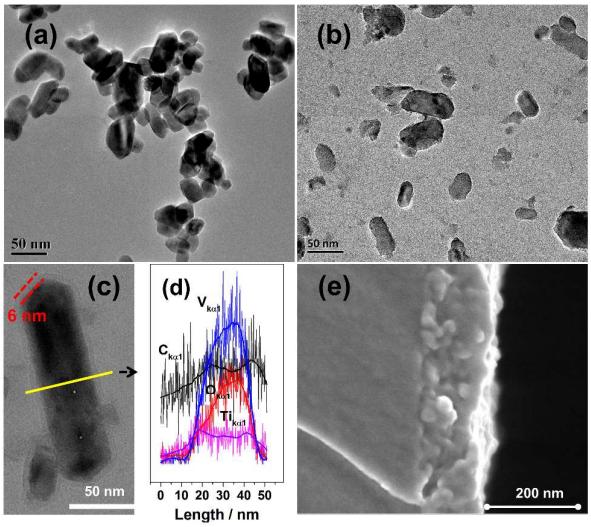

Figure 1.Surface-modified VO_2 NPs and the formed composite film. TEM images of VO_2 NPs before (a) and after (b) surface modification show that the aggregation of VO_2 NPs is reduced after surface modification; STEM image of single surface-modified VO_2 NPs (c) and the compositional scanning TEM curves (d), thin lines in (d) is the original data and thick lines are smoothed results of these original data (by Savitzky-Golay method, points of window: 65, polynomial order: 2), (c) and (d) show that VO_2 NPs are coated with a 6-nm-thick layer that shows higher contents of Ti and C, which may be polymers formed by titanium ethoxide; The cross-sectional SEM image of the formed composite film (e) shows that the film is homogeneous and consists of nanoparticles agglutinated by an amorphous substance.

3.2 Thermal analysis of xerogels and crystallisation of TiO_2(A)

Although this "two-step method" is more convenient for large-area preparation than the "annealing method" of VO_2 smart films, and the obtained films have advantages in mechanical strength and weatherability over I-I composite coatings, the advantages of TiO_2 have not been demonstrated because the TiO_2 in the films was uncrystallised. An annealing process is needed to crystallise the TiO_2 while keeping the thermochromic property of VO_2 (M/R). Thermoanalysis of the xerogel would clarify the reactions during annealing and would optimise the annealing process of the films.

TG-DTA and MS (CO_2 and H_2O) of TiO_2 xerogel show that decomposition of the organic components in the xerogel occurred at approximately 265 ºC (**Figure 2 a** shows a strong exothermic peak at 265 ºC in the DTA curve, followed by a peak at 285 ºC for H_2O and at 294 ºC for CO_2). The DTA and MS curves also indicate that decomposition of the organic components was incomplete under the testing conditions (10 ºC/min, in air) and that oxidation of the residual carbon continued to 530 ºC, which may cover up the TiO_2 crystallisation peak that should appear in this temperature range [31, 39, 40]. The XRD of the films annealed with different processes revealed that crystallisation of the TiO_2 xerogel starts at approximately 300 ºC (**Figure 2 b**). As shown in the figure, the crystallinity of TiO_2(A) increased as the annealing temperature increased, but it was less sensitive to the heating speed and holding time. In our experiments, annealing the samples with a longer holding time (T-A in **Figure 2 b**, 300 ºC for 2 hours) did not obviously increase the intensity of the XRD peaks, but the peaks' intensity could be easily increased by increasing the annealing temperature (T-B in **Figure 2 b**, 350 C for 30 min). Samples annealed with a quick heating rate and short holding time showed comparative intensity of XRD peaks, as seen for samples annealed at the same temperature (sample T-C1 and T-C2 in **Figure 2 b**, 400 C for 5 min and 30 min).

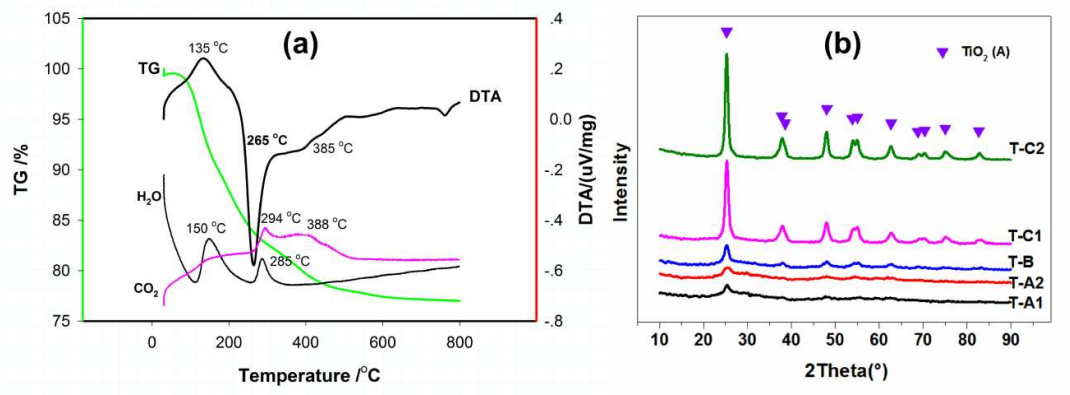

Figure 2. TG-DTA and mass spectrograph (CO_2 and H_2O) of TiO_2 xerogel (a) and XRD data of TiO_2 xerogel annealed with different annealing processes (b). Samples T-A1 and T-A2 were annealed at 10 ºC/min to 300 ºC for 30 min and 120 min, respectively; sample T-B was annealed at 10 ºC /min to 350 ºC for 30 min; and samples T-C1 and T-C2 were annealed at 10 ºC /min to 400 ºC for 5 min and 30 min, respectively. MS peaks of H_2O at 150 ºC indicate the release of absorbed water; the 285 ºC H_2O peak, combined with the 294 ºC CO_2 peak and the strong exothermic peak at 265 in the DTA curve indicate the decomposition of organic compounds; the continuous CO_2 peak from 300 C to 530 C indicates the oxidation of residual carbon.

It is known that new phase nucleation includes heterogeneous and homogeneous nucleation [41]. Heterogeneous nucleation usually occurs at the surface of the outer phase or at defects where lower activation energy of nucleus formation is required, but the number of nuclei is limited, and crystallisation is restricted by atomic diffusion; homogeneous nucleation requires much higher activation energy and sufficient nuclei for fast crystallisation. It could be inferred that, at higher annealing temperatures, homogeneous nucleation of TiO_2(A) was activated, and the speed of nucleation would jump to a extremely high level, while the diffusion of atoms has a **continuous** relationship with temperature[42], whose speed was increased continuous with temperature. Moreover, crystallised TiO_2 shows lower diffusion speed than amorphous TiO_2[17]. Based on these analyses, using a fast heating rate to a relatively high temperature and a shorter annealing time would favour TiO_2(A) crystallisation and restrict Ti diffusion.

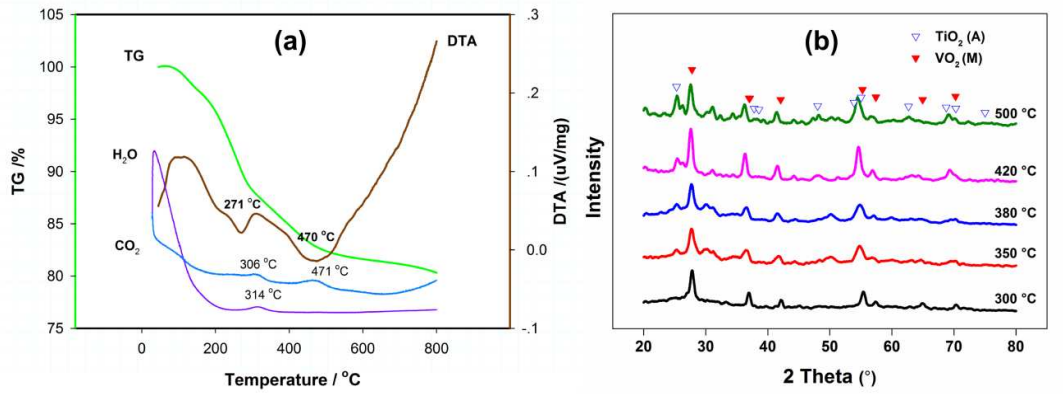

Figure 3. TG-DTA and mass spectrograph (CO_2 and H_2O) of TiO_2-VO_2 composite xerogels (a) and XRD of the gels annealed at different annealing temperatures (b) for 30 min. An exothermic peak appears in the DTA curve, combining with the CO_2 peak at 314 C and H_2O peak at 306, indicating the decomposition of organic

components around this temperature. Unlike the TiO_2 xerogel, a wide exothermic peak appears at approximately 470 C, and only CO_2 was detected around this temperature; considering the atmosphere was inert, there might be components (TiO_2 or VO_2) that are being reduced.

The TG-DTA and MS of TiO_2-VO_2 composite xerogel were taken in argon atmosphere (to prevent VO_2 from oxidising). Decomposition of organic components occurred at a similar temperature to that in TiO_2 xerogel (strong exothermic peak at 271 ºC in the DTA curve, an H_2O peak at 314 ºC and a CO_2 peak at 306 ºC). Because of the inert atmosphere, residual carbon remained until 470 ºC (a CO_2 peak appeared at 471 ºC, implying that an oxidation-reduction reaction may occur around this temperature). XRD of the xerogel showed a peak for TiO_2(A) (101) appeared after annealing at 400 ºC in argon. In fact, because the atmosphere was weakly reductive due to the decomposition of organic components, VO_2 NPs in the composite xerogel would lose their thermochromic property even at very low annealing temperatures in argon (280 ºC in our experiment). However, we found that due to the coated TiO_2 coating and VO_2 NPs' good crystallinity, the VO_2 NPs in the composite xerogel could maintain their thermochromic property for a short time in air at high temperature. DSC of the samples treated quickly in air (at 10 ºC/min to 300 ºC and quickly heated at a rate of 30 ºC/min to higher temperature, then quickly cooled to room temperature) showed that half of the thermochromic property could be maintained after quick heating to 400 ºC. XRD of these samples showed that the peaks for TiO_2(A) (101) could be observed above 350 ºC (**Figure 3, b**). As the annealing temperature increased, the peak intensity of both TiO_2(A) and V_2O_5 (PDF card: 41-1426) increased, and the VO_2 peak also shifted to lower angle. The increased peak intensity of TiO_2(A) and V_2O_5 indicates the crystallisation of TiO_2(A) and the oxidation of VO_2, while possible causes of the angle shift of VO_2 may be Ti doping[43], crystallisation of rutile TiO_2 (PDF card: 21-1276) or non-stoichiometry of VO_2, which was difficult to determine in this situation because of the uncertain atmosphere.

However, these results have already shown that TiO_2(A) and thermochromic VO_2 could coexist in the composite xerogel with a quick treatment process, indicating the probability of the existence of crystallised TiO_2(A)-VO_2 composite film.

3.3 Annealing of TiO_2-VO_2 composite films

Composite films were first annealed in argon at 10 ºC /min, the same rate as that used in the TG-DTA and MS tests. Because there were few total organic components in the films, the atmosphere would not change greatly, and the films' thermochromic property was likely to be maintained after annealing.

The results from the annealed composite films are slightly different from those of the composite xerogel. Crystallisation of TiO_2(A) films required a higher annealing temperature and only occurred in an annealing temperature range between 400 and 500 ºC. As the XRD results showed, the TiO_2(A) (101) peak was detected after sample was annealed at 450 ºC and disappeared above 500 ºC, which was higher than in pure TiO_2 film in comparison experiments. Heating hysteresis loops of the films show that their thermochromic property remained even after annealing at 550 ºC for 20 min, but their shapes and positions were changed. It has been reported that Ti-doping narrows hysteresis loops and increases the phase transition temperature (PTT)[44-46], thus the narrowed hysteresis loops may indicate the increased Ti-doping of VO_2 as the annealing temperature increased. However, the changes in the PTT did not follow the rules of Ti-doping. The PTT of the films first increased (450 ºC), then decreased (500 ºC) and increased again (550 ºC). Similar phenomena have been reported in Ti-doped pure VO_2 films, but there were differences in loop width changes.

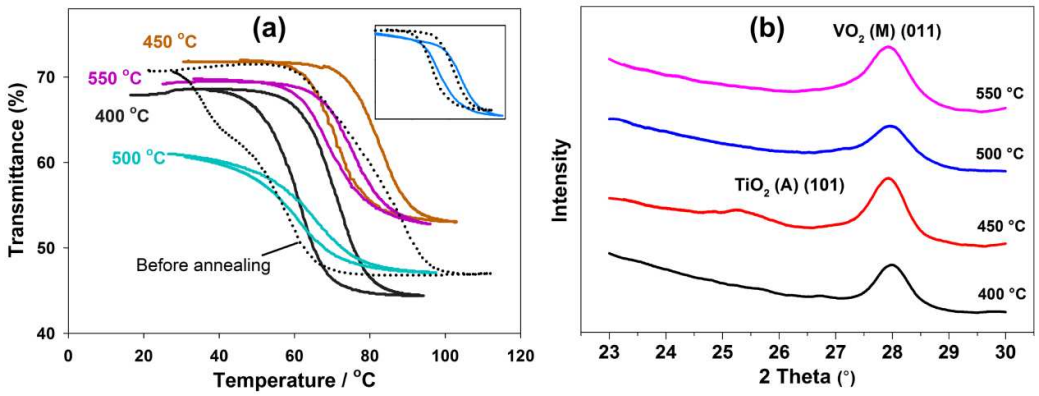

Figure 4. Heating hysteresis loops measured at 1500 nm (a) and XRD with 2θ from 23 ºC to 30 ºC (b) of films heated with different processes. Films were heated at 10 ºC/min to target temperatures (400, 450, 500 and 550 ºC) and held for 20 min in argon. The phase transition temperature (PTT) of the films first increased (450 ºC), then decreased (500 ºC) and then increased again (550 ºC), and the TiO_2 (A) (101) peak only appears in film annealed at 450 ºC. Inset in (a) shows the loops of film heated to 450 ºC for 20 min and film annealed with two-step annealing: 2 ºC/min to 300 ºC and quickly heated to 500 ºC at 30 ºC/min, then quickly cooled to room temperature. Film annealed with two-step annealing showed a narrower loop width (7.7 compared to 11.2 ºC) and higher transition temperature (78.7 compared to 76.7 ºC).

There might be other factors that influence the PTT during annealing. The most likely factor is non-stoichiometry of VO_2. Non-stoichiometry of VO_2 would decrease the PTT and hysteresis loop width of VO_2 (but not as effectively as would Ti-doping)[47]. As shown in the TG-DTA and MS results (**Figure 3 a**), CO_2 was detected at approximately 470 ºC, indicating that there were components being reduced around this temperature. The strong reducing property of carbon could change the stoichiometry of VO_2 NPs. This was confirmed by experiment. It was shown that a lower heating rate at low temperature was favourable for the volatilisation of organic components and the reducing the residual carbon in the composite film, and a higher heating rate at high temperature would shorten the time of the reducing reaction. Thus, a film treated with this annealing process (two-step annealing, 2 ºC/min to 300 ºC and quick heating to 500 ºC at 30 ºC/min then quick cooling to room temperature) was prepared. As expected, compared to film annealed at 450 ºC for 20 min at 10 ºC/min, this film had a higher doping content of Ti, which was inferred from the slightly narrowed loop width and the slightly increased PTT that was consistent with this change.

As mentioned above, a quick annealing process at a relatively high temperature could create enough undercooling degrees for TiO_2(A) crystallisation, but the XRD peak of TiO_2(A) (101) still disappeared with this fast annealing process. The reasons for this phenomenon were uncertain; most likely, the crystallisation of TiO_2(A) was restricted by VO_2 at this temperature range because we found later that mesoporous films had a wider temperature range for TiO_2(A) crystallisation. In any case, TiO_2-VO_2 composite films with crystallised TiO_2(A) could be prepared, although a specific annealing temperature range (between 400 and 500 ºC) was required.

3.4 Influence of annealing on the optical performance of TiO_2-VO_2 composite film

Films with different heating schedules have been described above, and we have already shown that the heating schedule would influence organic component release and TiO_2(A) crystallisation. Additionally,

the heating schedule also influenced the films' porosity, which affected the optical performance of the composite films[48].

During film annealing, two changes occurred: mass loss and crystallisation. Mass loss was induced by decomposition of the remaining organic components and the condensation reaction of uncrystallised TiO_2. This led to film contraction, while crystallisation strengthened the film and inhibited film contraction. According to this analysis, film densification would be accelerated when crystallisation occurred long after the films' contraction. As showed by TG (**Figure 3 a**), the largest mass loss of the TiO_2-VO_2 composite films was induced by the decomposition of organic components (approximately 10%) at approximately 270 ºC, while TiO_2(A) crystallisation occurred above 300 ºC (**Figure 2 a**); thus, film densification had been accelerated in our experiments. However, it has been reported that heating rate can reduce crystallisation temperatures[49]. Due to crystallisation, the films would have grown strong enough to counteract the film contraction at the lower heating rate.

Film density can be characterised by reflectance. For mesoporous materials **with different porosity**, the maximum reflectance value is proportional to the density[50]. The reflectances of films annealed at different heating rates are shown in **Figure 5**. According to the maximum reflectance, the order of film densities could be concluded to be the following: 10 ºC/min to 300 ºC < 10 ºC/min to 500 ºC < 2 ºC/min to 300 ºC <two-step annealing. As predicted, films annealed at lower heating rates had higher porosity. We also observed that the films annealed at higher temperatures had lower density. This finding indicates that, at higher temperature, the films were strong enough to withstand the film contraction induced by mass loss, and a low heating rate was not required at high temperature.

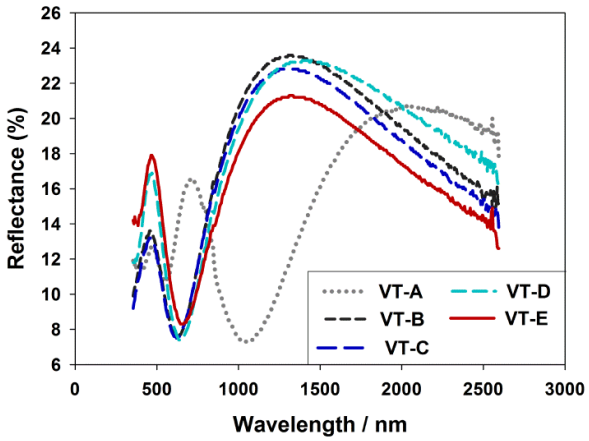

Figure 5. Room temperature reflectance of films annealed with different processes. VT-A: before annealing, VT-B: 10 ºC/min to 300 ºC for 20 min, VT-C: 2 ºC /min to 300 ºC for 20 min, VT-D: 10 ºC/min to 500 ºC for 20 min and VT-E: 2 ºC /min to 300 ºC and 30 ºC/min to 500 ºC, then quickly cooled (two-step annealing). Maximum reflectance is proportionate to film density, and the order of film densities could be concluded as follows: 10 ºC/min to 300 ºC < 10 ºC/min to 500 ºC < 2 ºC/min to 300 ºC <two-step annealing. The film before annealing has the lowest density, indicating that all films contracted during annealing.

Low density means high porosity. Porosity can improve both luminous transmittance (T_{lum}) and solar energy modification ability (ΔT_{sol}). Values for the T_{lum} and ΔT_{sol} of the films are shown in **Table 1.** As mentioned above, the film without annealing shows comparable optical performance to pure VO_2 film prepared by a solution process: T_{lum}=50 %, ΔT_{sol}=7.1 %[32, 51]. Film annealed at 2 ºC/min has higher T_{lum} and ΔT_{sol} (T_{lum}=58.5 % and ΔT_{sol} =7.4 %) values than film annealed at 10 ºC/min (T_{lum}=53.4 % and ΔT_{sol}

=6.2 %). Film annealed at 500 ºC showed better optical performance than film annealed at 300 ºC. The best results were obtained for film treated with two-step annealing (T_{lum}=61.6%, ΔT_{sol}= 8.2%). These results confirmed the influence of annealing process that had been inferred above.

Table 1. Luminous transmittance (T_{lum}) and solar energy modification ability (ΔT_{sol}) of films annealed with different processes

P123		Room Temperature	10 ºC/min to 300 ºC	10 ºC/min to 500 ºC	2 ºC/min to 300 ºC	Two-step annealing
T_{lum} (%)	20 ºC	63.4	53.4	58.5	58.5	61.6
	90 ºC	63.8	53.9	56.5	56.5	59.2
ΔT_{sol} (%)		6.9	6.2	5.8	7.4	8.2

3.4 Mesoporous VO_2-TiO_2 composite film

The results above have already shown the advantage of porosity for the optical performance of films. Although the porosity of the films could be regulated by the heating rate, the degree of regulation is limited. To further increase the optical performance, we used a method for construction of a mesoporous structure[52]. P123 was used as a precursor in our mesopores composite films. The decomposition temperature of this copolymer template is below 280 ºC. According to the literature, a slow heating rate to 300 ºC would both help remove P123 and preserve the mesoporous structure[52].

Films were prepared at different heating rates and with different amounts of P123. **Table 2** shows the T_{lum} and ΔT_{sol} of films with different amounts of P123 that were annealed at 300 ºC using different heating rates. Generally speaking, the difference in T_{lum} between films heated at 2 ºC/min and at 10 ºC/min is smaller than that in films without P123 because the film strength during annealing was reduced after adding P123. However, there are differences in the performance of the films. Films with 1% and 4% P123 show higher T_{lum} at 2 ºC/min than 10 ºC/min, but the film with 2% P123 shows the opposite result and has the lowest T_{lum} (approximately 52%) at 2 ºC/min. Moreover, the relationship between ΔT_{sol} and film density was not as clear as expected; for example, the film with 4% P123 should have higher ΔT_{sol} at 2 ºC/min than 10 ºC/min because of the lower density at 2 ºC/min, but it did not.

It should be mentioned that annealing films with P123 was slightly different than performing the process without P123. With regard to the change in film microstructure, introduced mesopores would reduce the films' strength, which was favourable for film contraction and improvement of the film density, but pore-wall contraction would also occur as the porosity increased, which would increase pore diameter and reduce film density[53]. These two changes would lead to differences among films with different amounts of P123 during annealing because the amount of P123 influences the pore structure of the films[53]. Regarding the optical properties, the degrees of film thickness and density change of films with and without P123 would create light interference difference between the film interfaces. Films with P123 have larger changes in film thickness and density because of their higher mass loss, which would lead to remarkable changes in reflection induced by interference. Previous work has shown that interference at these interfaces could modify the T_{lum} and ΔT_{sol} of VO_2 films[54], which we called self-antireflection (AR). This effect is particularly obvious in the 2% P123 film (**S2**).

Interference occurs in any thin films with smooth interfaces, and the optical performance of our films could be further improved by optimising their thickness. However, for single-layer films, the improvement of performance though interference is not as obvious as that produced by porosity[48, 54]. As the content of P123 increased, the reflectance of interfaces was lowered, and porosity played the main role in optical

performance improvement.

Table 2. Luminous transmittance (T_{lum}) and solar energy modification ability (ΔT_{sol}) of films with different amounts of P123 annealed with different processes

		Room temperature			2 ºC/min to 300 ºC			10 ºC/min to 300 ºC			Two-step annealing	
P123		1%	2%	4%	1%	2%	4%	1%	2%	4%	2%	4%
T_{lum} (%)	20 ºC	64.4	63.0	66.4	57.0	52.7	60.9	55.3	57.4	58.3	60.4	62.8
	90 ºC	63.4	60.0	65.1	55.4	51.7	60.8	54.0	56.3	57.6	58.8	62.5
ΔT_{sol} (%)		9.1	13.3	9.8	6.6	9.7	8.9	7.0	7.0	9.9	8.4	10.7

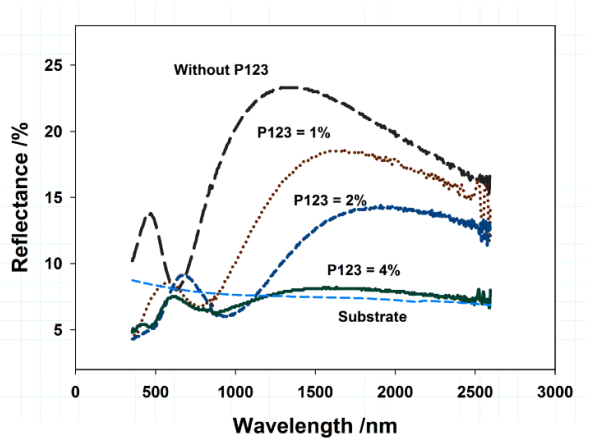

Figure 6. Room temperature reflectance of films containing different amounts of P123 (wt%). As the amount of P123 increased, the film reflectance decreased. The reflectance of film with 4% P123 was decreased to a level lower than that of the substrate.

As shown in **Figure 6**, the reflectance of film with 4% P123 was reduced to a very low level (even lower than that of the substrate). Estimation using the Lorentz-Lorenz relationship showed that the porosity of the composite film may exceed 50%[25, 54]. Mesopores in the film created by P123 not only increased as the amount of P123 increased but also get uniformly distributed. This is because ordered structure usually forms at high concentrations of surfactant[53]. SEM analysis of film (**Figure 6**) with 4% P123 annealed by two-step annealing shows that the film surface was full of uniformly distributed mesopores with diameters of 5-7 nm. The cross-section of the film shows that the mesopores are uniformly distributed in the films as well. Although there were cracks in the films, most of their sizes were less than 300 nm, shorter than visible wavelength, and would not influence the films' optical performance. The cracks may be reduced by procedures that have been studied by other researchers[55], and we will study this in future work. Because the reflectance of the 4% P123 film was reduced to a very low level, these films could be treated as absorption films; that is, their optical performance is dependent on their thickness[32]. The optical performance of VO_2-based absorption films could be further improved by increasing the film thickness, but the thickness of the composite film could not be increased infinitely because the inorganic film would crack during film contraction. The film with best optical performance we have prepared has a film thickness (**Figure 8**) of 500-600 nm. The T_{lum} and ΔT_{sol} are 62.0 % (20 ºC), 60.5 % (90 ºC) and 14.6 %, respectively, better than any reported VO_2-based inorganic thermochromic films[32] and much better than that of reported nanoporous VO_2 films at the same T_{lum} (ΔT_{sol} =6.4 % when T_{lum} is approximately 60 %)[48].

We could not make a comparison of ΔT_{sol} between our experiment and calculated results, as we did in O-I coatings, mainly because the thickness of I-I films is limited. At the similar transmittance and film thickness, the caculated ΔT_{sol} is approximate 17 % (**S1**). This value is comparable to that of O-I coatings.

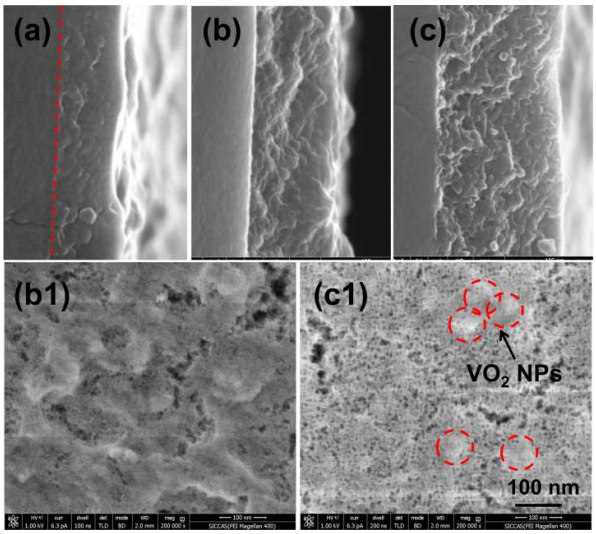

Figure 7. SEM images of films containing different amounts of P123 (wt%). (a), (b) and (c) are cross-sections of film without P123 and with 2 % P123 and 4% P123, respectively. (b1) and (c1) are the surfaces of film with 2% and 4% P123, respectively. Films without P123 are compact and few pores can be observed (a); cross-section of 2% P123 (b) is not smooth due to inhomogeneous distribution of mesopores, which is clearly shown in the surface image (b1); the 4% p123 film showed a smooth cross-section (c) and homogeneous distribution of mesopores (c1), and the surface image also shows that the 4% P123 film has a high concentration of mesopores.

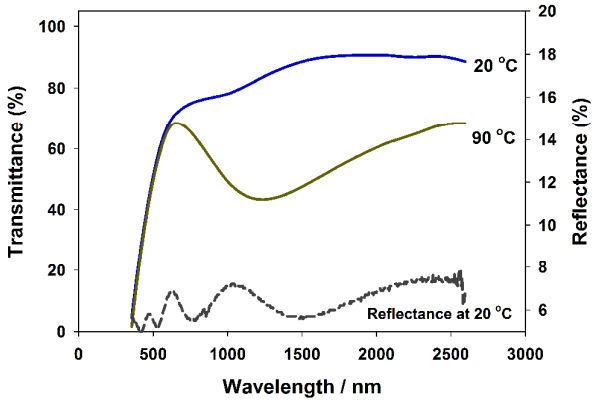

Figure 8. Transmittance and room temperature reflectance of the best sample. Reflectance curve shows clear valleys induced by interference. Film thickness is estimated to be aproximate twice as thick as the 4% P123 sample in **Figure 6** (about 270 nm measured by SEM in **Figure 7**, details see **S3**) according the the reflectance curve[54].

The heating hysteresis loops of films with 4% P123 are shown in **Figure 9**. Unlike in film without P123, the properties of VO_2 NPs in the 4% P123 film were maintained at higher temperature. The loop of this film annealed at 400 ºC for 20 min is almost the same as that of films without annealing. The loop

widths of films annealed at higher temperature are also wider than that of film without P123. XRD shows that TiO_2(A) (101) appeared after annealing at 500 ºC for 20 min and increased as the annealing temperature increased. This phenomenon was consistent with reports that mesoporous TiO_2 films show lower crystallinity compared to nonporous films because the cross-links between the nano-building blocks of the block copolymer retard the crystallisation of TiO_2 during annealing[52]. The film with two-step annealing shows higher peak intensity of TiO_2(A) (101), most likely because the slow heating speed at the lower temperature favoured elimination of the block copolymer. The loop width for the film with two-step annealing was also wider because the short time at the higher temperature reduces the Ti diffusion to VO_2 NPs.

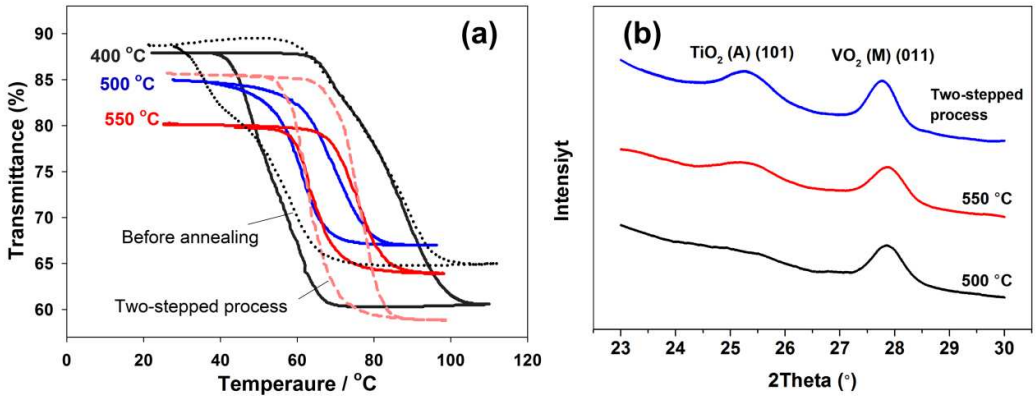

Figure 9. Heating hysteresis loops measured at 1500 nm (a) and XRD with 2θ from 23 º to 30 º (b) of films with 4% P123 annealed with different processes (10 ºC/min to target temperature and held for 20 min or two-step annealing). The film annealed at 400 C for 20 min has comparable loop width (31.1 ºC compare to 29.2 ºC) and transition temperature (69.1 ºC compare to 66.5 ºC) with films before annealing, indicating that the addition of P123 would delay the influence of TiO_2 sol on the VO_2 thermochromic property. The loop width and transition temperature of films annealed at 500 ºC, 550 ºC for 20 min and with two-step annealing are 8.7, 11.4, 13 ºC and 64.7, 69.9, 69.3 ºC, respectively. The unusual performance of the film annealed at 500 ºC may be caused by non-stoichiometry, which has been discussed above, because it shows a lowered transition temperature. The film treated with two-step annealing shows wider loop width and a lower transition temperature as expected, and it also has the highest peak intensity for TiO_2 (A) (101).

3.5 Self-cleaning properties of mesoporous VO_2-TiO_2 composite film

Self-cleaning properties in thin films usually require low water contact angles and photocatalytic decomposition of organic contaminants. The low water contact angle is necessary for rainwater to clear surface dust off the films. The sample without annealing has the highest contact angle because of the remaining organic compounds. As the annealing temperature increased, the contact angle decreased due to the decomposition of organic compounds (**Table 3**). The mesoporous films showed lower contact angle values than that of films without mesopores. This could be caused partly by their higher surface roughnesses[56, 57, 58] and partly by their less residual carbon (residual carbon could be removed easily from mesoporous films). The lowest contact angle (less than 5 º) was obtained on the sample with the highest TiO_2(A) (101) peak intensity. Thus the crystallinity of TiO_2(A) may be responsible for the low contact angle.

Table 3. Contact angle of films with and without P123 annealed at different temperatures with two-step annealing

	Before annealing	Without P123			4% P123		
		300 ºC	400 ºC	500 ºC	300 ºC	400 ºC	500 ºC
Contact angle	74 º	56 º	47 º	37 º	35 º	19 º	5 º
Ra (nm)	-	44.2	38.1	41.7	87.8	93.1	97.2

The photocatalytic ability to decompose organic contaminants was characterised by performing organic contaminant (methylene blue, MB) removal under UV irradiation. Decomposition of MB by the films was monitored by measuring the amount of remaining MB on the coatings after UV irradiation as a function of time[57]. Three samples were compared: a sample with 4% P123, a sample without P123 and a black substrate. The UV irradiation used in our experiment is stronger than reported[56], and MB would decompose under this UV irradiation without catalysis. As shown in **Figure 10**, the decomposition of MB on the fused-silica substrate under UV irradiation was fast at the beginning, but the remaining MB was stable for a long time. This likely occurred because there was much less MB adsorbed on the quartz glass than on the other samples (**S4**), and the surface MB was quickly decomposed under UV irradiation; however, the fused-silica substrate but there has no photocatalytic ability for the fused-silica substrate, and the decomposition of the remaining MB was slowed. The other two samples had comparable absorption of MB. Both samples showed relatively fast MB decomposition until it was completely decomposed, indicating the existence of photocatalytic ability. As expected, the sample with 4% P123 that was annealed with two-step annealing showed better ability to remove MB, taking only half the time of the sample without P123. Both the higher content of TiO_2(A) and the mesoporous structure may account for this efficiency. Systematic studies of the photocatalytic ability of these composite films are in progress.

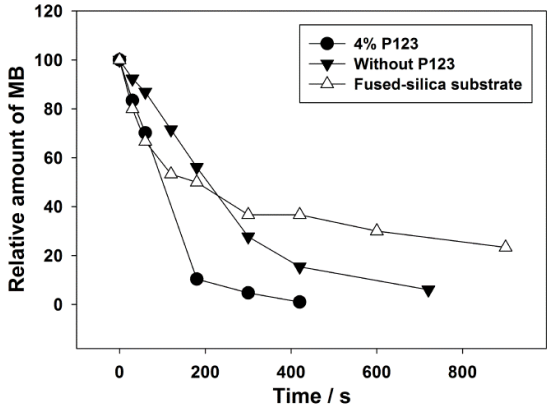

Figure 10. Comparison of the photocatalytic properties of a sample with 4% P123, a sample without P123 and a black substrate. The sample with 4% P123 was annealed with two-step annealing, and the sample without P123 was annealed at 10 ºC/min to 450 ºC for 20 min. The self-cleaning properties of composite films were determined by the relative amount of methylene blue (MB) remaining after UV irradiation.

4. Conclusions

Crystallised TiO_2(A)-VO_2(M/R) composite films have been prepared by dispersing VO_2 NPs in TiO_2 sol and annealing with an optimised two-step annealing process. The optical performance of these composite films could be improved by increasing their porosity through controlling the annealing rate or by introducing mesopores. The best-performing sample we obtained has a T_{lum}= 62.0 % (20 ºC), 60.5 %

(90 ºC) and ΔT_{sol} = 14.6 %, better than any reported VO_2-based inorganic films. These composite films show self-cleaning properties (low contact angle and photocatalytic ability), which is an important function for the practical usage of smart windows. Moreover, because of the good film-forming property, this method for preparing VO_2-based films would open a route for solution-based VO_2 multilayer preparation as had been achieved by reactive DC magnetron sputtering[22]. Future work will focus on further improving the optical performance and self-cleaning properties of the composite films.

Acknowledgements

This study was supported in part by funds from MOST (2014AA032802), NSFC (State Outstanding Young Scholars, 51325203) and Innovation Program of Shanghai Municipal Education Commission (14ZZ099).

References

1. P. Jin and S. Tanemura, *Jpn. J. Appl. Phys. Part 1 - Regul. Pap. Short Notes Rev. Pap.*, **1994**, 33, 1478-1483.
2. P. Jin, G. Xu, M. Tazawa and K. Yoshimura, *Appl. Phys. A-Mater.*, **2003**, 77, 455-459.
3. Y. Gao, H. Luo, Z. Zhang, L. Kang, Z. Chen, J. Du, M. Kanehira and C. Cao, *Nano Energy*, **2012**, 1, 221-246.
4. S. M. Babulanam, T. S. Eriksson, G. A. Niklasson and C. G. Granqvist, *Solar Energy Materials*, **1987**, 16, 347-363.
5. C. G. Granqvist, P. C. Lansåker, N. R. Mlyuka, G. A. Niklasson and E. Avendaño, *Sol. Energy Mater. Sol. Cells* **2009**, 93, 2032-2039.
6. M. D. Hernández-Alonso, F. Fresno, S. Suárez and J. M. Coronado, *Energy & Environmental Science*, **2009**, 2, 1231.
7. M. R. Hoffmann, S. T. Martin, W. Y. Choi and D. W. Bahnemann, *Chem. Rev.*, **1995**, 95, 69-96.
8. M. A. Henderson, *Surf. Sci. Rep.*, **2011**, 66, 185-297.
9. A. Di Paola, E. Garcia-Lopez, G. Marci and L. Palmisano, *Journal of Hazardous Materials*, **2012**, 211, 3-29.
10. R. Asahi, T. Morikawa, T. Ohwaki, K. Aoki and Y. Taga, *Science*, **2001**, 293, 269-271.
11. M. Hervieu, *Adv. Mater.* , **1995**, 7, 91-92.
12. M. Della Negra, M. Sambi and G. Granozzi, *Surf. Sci.* , **2001**, 494, 213-228.
13. Y. Muraoka and Z. Hiroi, *Appl. Phys. Lett.* , **2002**, 80, 583-585.
14. Z. Hiroi, T. Yamauchi, Y. Muraoka, T. Muramatsu and J. I. Yamaura, *J. Phys. Soc. Jpn.* , **2003**, 72, 3049-3052.
15. K. Okazaki, H. Wadati, A. Fujimori, M. Onoda, Y. Muraoka and Z. Hiroi, *Phys. Rev. B*, **2004**, 69.
16. R. Eguchi, S. Shin, A. Fukushima, T. Kiss, T. Shimojima, Y. Muraoka and Z. Hiroi, *Appl. Phys. Lett.* , **2005**, 87.
17. Z. T. Zhang, Y. F. Gao, L. T. Kang, J. Du and H. J. Luo, *J. Phys. Chem. C* **2010**, 114, 22214-22220.
18. G. Fu, A. Polity, N. Volbers and B. K. Meyer, *Thin Solid Films* **2006**, 515, 2519-2522.
19. Y. B. Zhang, W. X. Huang, L. W. Song, J. Z. Yan, Q. W. Shi and Y. Zhang, *J. Inorg. Mater.*, **2013**, 28, 229-234.
20. K. Nagashima, T. Yanagida, H. Tanaka and T. Kawai, *J. Appl. Phys.* , **2007**, 101, -.
21. Y. Muraoka, Y. Ueda and Z. Hiroi, *8th ISSP International Symposium on Correlated Electrons (ISSP-Kashiwa 2001)*, **2001**, 965-967.
22. N. R. Mlyuka, G. A. Niklasson and C. G. Granqvist, *Phys. Status Solidi A*, **2009**, 206, 2155-2160.

23. P. Evans, M. E. Pemble, D. W. Sheel and H. M. Yates, *Journal of Photochemistry and Photobiology a-Chemistry*, **2007**, 189, 387-397.
24. P. Jin, G. Xu, M. Tazawa and K. Yoshimura, *Jpn. J. Appl. Phys., Part 2* **2002**, 41, L278-L280.
25. S. Y. Li, G. A. Niklasson and C. G. Granqvist, *J. Appl. Phys.* , **2010**, 108.
26. H. Kakiuchida, P. Jin and M. Tazawa, *Thin Solid Films* **2008**, 516, 4563-4567.
27. U. Qureshi, T. D. Manning, C. Blackman and I. P. Parkin, *Polyhedron*, **2006**, 25, 334-338.
28. U. Qureshi, T. D. Manning and I. P. Parkin, *J. Mater. Chem.* , **2004**, 14, 1190-1194.
29. J. Du, Y. F. Gao, H. J. Luo, L. T. Kang, Z. T. Zhang, Z. Chen and C. X. Cao, *Sol. Energy Mater. Sol. Cells* **2011**, 95, 469-475.
30. I. Balberg, B. Abeles and Y. Arie, *Thin Solid Films* **1974**, 24, 307-310.
31. R. Li, S. D. Ji, Y. M. Li, Y. F. Gao, H. J. Luo and P. Jin, *Mater. Lett.* , **2013**, 110, 241-244.
32. Z. Chen, Y. Gao, L. Kang, C. Cao, S. Chen and H. Luo, *Journal of Materials Chemistry A*, **2014**, 2, 2718-2727.
33. Y. F. Gao, S. B. Wang, H. J. Luo, L. Dai, C. X. Cao, Y. L. Liu, Z. Chen and M. Kanehira, *Energy Environ. Sci.* , **2012**, 5, 6104-6110.
34. L. H. Hoang, P. V. Hai, P. V. Hanh, N. H. Hai, X. B. Chen and I. S. Yang, *Materials Letters*, **2011**, 65, 3047-3050.
35. B. M. Reddy, E. P. Reddy and S. Mehdi, *Materials Chemistry and Physics*, **1994**, 36, 276-281.
36. M. Burgos and M. Langlet, *Thin Solid Films*, **1999**, 349, 19-23.
37. J. Lin, J. A. Siddiqui and R. M. Ottenbrite, *Polym. Adv. Technol.*, **2001**, 12, 285-292.
38. G. D. Parfitt, *Pure Appl. Chem.* , **1976**, 48, 415-418.
39. D. Dambournet, I. Belharouak and K. Amine, *Chemistry of Materials*, **2010**, 22, 1173-1179.
40. H. J. Nam, T. Amemiya, M. Murabayashi and K. Toh, *Journal of Physical Chemistry B*, **2004**, 108, 8254-8259.
41. R. Lopez, T. E. Haynes, L. A. Boatner, L. C. Feldman and R. F. Haglund, *Phys. Rev. B*, **2002**, 65, -.
42. J. D. Mcbrayer, R. M. Swanson and T. W. Sigmon, *J. Electrochem. Soc.* , **1986**, 133, 1242-1246.
43. Y. M. Li, S. D. Ji, Y. F. Gao, H. J. Luo and M. Kanehira, *Sci. Rep.*, **2013**, 3.
44. F. Beteille, R. Morineau, J. Livage and M. Nagano, *Mater. Res. Bull.* , **1997**, 32, 1109-1117.
45. M. Nishikawa, T. Nakajima, T. Kumagai, T. Okutani and T. Tsuchiya, *J. Ceram. Soc. Jpn.* , **2011**, 119, 577-580.
46. M. Nishikawa, T. Nakajima, T. Kumagai, T. Okutani and T. Tsuchiya, *Jpn. J. Appl. Phys.*, **2011**, 50, 5.
47. Griffith.Ch and H. K. Eastwood, *J. Appl. Phys.* , **1974**, 45, 2201-2206.
48. L. Kang, Y. Gao, H. Luo, Z. Chen, J. Du and Z. Zhang, *ACS Appl. Mat. Interfaces* **2011**, 3, 135-138.
49. J. D. Bass, D. Grosso, C. Boissiere and C. Sanchez, *J Am Chem Soc*, **2008**, 130, 7882-7897.
50. M. Houmard, D. Riassetto, F. Roussel, A. Bourgeois, G. Berthome, J. C. Joud and M. Langlet, Surf. Sci. , 2008, 602, 3364-3374.
51. Z. T. Zhang, Y. F. Gao, Z. Chen, J. Du, C. X. Cao, L. T. Kang and H. J. Luo, *Langmuir*, **2010**, 26, 10738-10744.
52. J. H. Pan, X. S. Zhao and W. I. Lee, *Chemical Engineering Journal*, **2011**, 170, 363-380.
53. D. Grosso, F. Cagnol, G. Soler-Illia, E. L. Crepaldi, H. Amenitsch, A. Brunet-Bruneau, A. Bourgeois and C. Sanchez, *Adv. Funct. Mater.*, **2004**, 14, 309-322.
54. Z. Chen, Y. F. Gao, L. T. Kang, J. Du, Z. T. Zhang, H. J. Luo, H. Y. Miao and G. Q. Tan, *Sol. Energy Mater. Sol. Cells* **2011**, 95, 2677-2684.
55. K. S. Jang, M. G. Song, S. H. Cho and J. D. Kim, *Chem. Commun.*, **2004**, DOI: 10.1039/b404409f,

1514-1515.

56. R. N. Wenzel, *Industrial and Engineering Chemistry*, **1936**, 28, 988-994.
57. D. Lee, M. F. Rubner and R. E. Cohen, *Nano Lett.*, **2006**, 6, 2305-2312.
58. N. Stevens, C. I. Priest, R. Sedev and J. Ralston, *Langmuir*, **2003**, 19, 3272-3275.

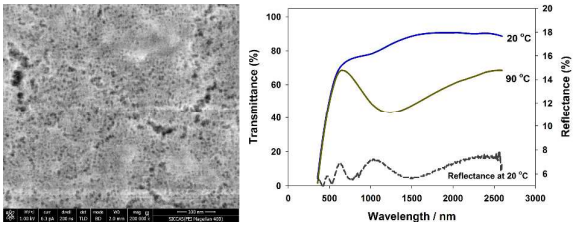

A "two-step" method was developed for preparation of crystallised TiO_2(A)-VO_2(M/R) nanocomposite mesoporous films with self-cleaning properties and excellent thermochromic performance.